The Relationship of Weddell Polynya and Open-Ocean Deep Convection to the Southern Hemisphere Westerlies

WOO GEUN CHEON

The 6th R&D Institute-1, Agency for Defense Development, Jinhae, South Korea

YOUNG-GYU PARK

Ocean Circulation and Climate Research Division, Korea Institute of Ocean Science and Technology, Ansan, South Korea

J. R. TOGGWEILER

NOAA/Geophysical Fluid Dynamics Laboratory, Princeton, New Jersey

SANG-KI LEE

Cooperative Institute for Marine and Atmospheric Studies, University of Miami, and NOAA/Atlantic Oceanographic and Meteorological Laboratory, Miami, Florida

(Manuscript received 26 May 2013, in final form 3 October 2013)

ABSTRACT

The Weddell Polynya of the mid-1970s is simulated in an energy balance model (EBM) sea ice–ocean coupled general circulation model (GCM) with an abrupt 20% increase in the intensity of Southern Hemisphere (SH) westerlies. This small upshift of applied wind stress is viewed as a stand in for the stronger zonal winds that developed in the mid-1970s following a long interval of relatively weak zonal winds between 1954 and 1972. Following the strengthening of the westerlies in this model, the cyclonic Weddell gyre intensifies, raising relatively warm Weddell Sea Deep Water to the surface. The raised warm water then melts sea ice or prevents it from forming to produce the Weddell Polynya. Within the polynya, large heat loss to the air causes surface water to become cold and sink to the bottom via open-ocean deep convection. Thus, the underlying layers cool down, the warm water supply to the surface eventually stops, and the polynya cannot be maintained anymore. During the 100-yr-long model simulation, two Weddell Polynya events are observed. The second one occurs a few years after the first one disappears; it is much weaker and persists for less time than the first one because the underlying layer is cooler. Based on these model simulations, the authors hypothesize that the Weddell Polynya and open-ocean deep convection were responses to the stronger SH westerlies that followed a prolonged weak phase of the southern annular mode.

1. Introduction

From 1974 to 1976, a persistent large-scale open-ocean polynya was observed in the Weddell Sea by scanning passive microwave sensors on polar-orbiting satellites (Zwally and Gloersen 1977; Carsey 1980; Gordon and Comiso 1988). This polynya, termed the "Weddell Polynya," was situated far off the Antarctic coast, west of the Greenwich meridian. The ice-enclosed open-water area of the polynya was observed throughout the period, except from late spring to early fall when sea ice in this region is routinely absent (Carsey 1980). Martinson et al. (1981) proposed a vertical redistribution of heat with weak horizontal variation as a triggering factor for the Weddell Polynya. They also argued that a transient feature, rather than the mean atmospheric and oceanic circulations, must be responsible for this polynya's occurrence because the maximum divergence areas of the atmosphere and ocean in the Weddell Sea do not correspond to the observed polynya area. Comparing hydrographic station data, Gordon (1982) revealed that the Weddell Sea Deep Water (WSDW) extending from about 200 to 2700 m beneath the observed Weddell Polynya became significantly

Corresponding author address: Young-Gyu Park, Ocean Circulation and Climate Research Division, Korea Institute of Ocean Science and Technology, 787 Hean-ro(st), Sangnok-gu, Ansan, South Korea.
E-mail: ypark@kordi.re.kr

colder and fresher in 1976–78 than in 1973. This suggests that full-scale open-ocean deep convection giving rise to the so-called Weddell chimney (Killworth 1979) occurred after the first opening of the Weddell Polynya in 1974.

The whole process, from the preconditioning to the open-ocean deep convection, consists of four stages. In the first stage, a large area of the pycnocline is raised over a large area so that the warm and salty WSDW lies just below the cold fresh surface layer above. In the second stage, the warmth of the upwelled WSDW thermodynamically generates the Weddell Polynya by hindering new sea ice formation or by melting existing sea ice (Martinson et al. 1981). In the third stage, relatively warm surface water in the large-scale ice-free ocean area surrounded by sea ice is brought in direct contact with extremely cold air and is thus transformed to sea ice. The ensuing brine rejection, combined with the relatively high salinity of the upwelled WSDW, acts to destabilize the whole water column, generating and maintaining open-ocean deep convection (Gordon 1982; Killworth 1983). On the other hand, the warmth of the WSDW injected into the surface layer periodically restores stratification of the water column by slowing down sea ice formation. Such an oscillatory mode is inherent in the formation process of open-ocean polynyas (Gordon 1991; Goosse and Fichefet 2001). In the final stage, the multiyear persisting large-scale polynya disappears when the upwelled water is no longer warm enough to melt the sea ice, which is a part of the results derived from this study and is described in the following.

So what generates the preconditions for the Weddell Polynya in the first stage? Martinson et al. (1981) first speculated that larger-than-normal salt rejection due to the anomalous formation of sea ice is the cause for this. Using observational data, Gordon et al. (2007) made an attempt to connect it with major climate modes of variability. They presented a hypothesis that drier-than-normal air that the Weddell Sea experienced during the prolonged negative phase of the southern annular mode (SAM) and increased sea ice formation due to colder-than-normal conditions in the polynya area under La Niña conditions can generate the preconditions for the Weddell Polynya. At some point these conditions result in small-scale overturning, leading to upwelling of the WSDW. It should be noted that small-scale overturning is distinct from open-ocean deep convection in the third stage because the Weddell chimney occurred after the first occurrence of the Weddell Polynya as discussed earlier. A topographic effect of Maud Rise was also studied as the preconditioning factor (Ou 1991; Alverson and Owens 1996; Holland 2001).

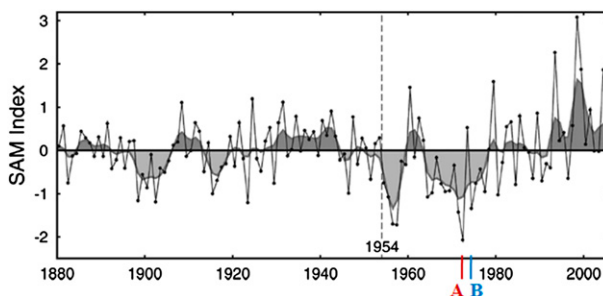Here, we present and explore a possible link between the SAM and the Weddell Polynya. The observed

FIG. 1. SAM time series based on SLP indices for various sectors of the SO. Yearly values are shown as the black line connecting annual values. The thicker gray line and gray shading denote the 5-yr low-pass-filtered data. This figure is quoted from Fig. 4 of Gordon et al. (2007). The red character A is indicative of 1972 when the negative phase of the SAM reached its peak, and the blue character B is indicative of 1974 when the Weddell Polynya first occurred.

Weddell Polynya first occurred in 1974 (marked with blue character B), which was 2 years after the SAM [SAM index is based on sea level pressure (SLP) data as shown in Fig. 1] reached a minimum in 1972 (marked with red character A). That is, the Weddell Polynya formed in a transition period when the weakened Southern Hemisphere (SH) westerlies began to regain strength. This suggests another important candidate mechanism for preconditioning the Weddell Polynya (i.e., strengthening of the SH westerlies).

The Antarctic continent is dominated by an overlying yearlong high pressure center and is continuously surrounded by several low pressure systems. The northern part of the Southern Ocean (SO) is dominated by the SH westerlies, while its southern part is dominated by easterly winds and strong offshore katabatic winds (Wadhams 2000). The Weddell gyre controls the influx of relatively warm, salty Circumpolar Deep Water (CDW) into the interior of the Weddell Sea (Orsi et al. 1993), and its northern limb is in contact with the Antarctic Circumpolar Current (ACC), the intensity of which is barotropically and baroclinically linked with the SH westerlies (Cai and Baines 1996; McDermott 1996; Gnanadesikan and Hallberg 2000; Gent et al. 2001). Moreover, according to the analysis of hydrographic data (Orsi et al. 1993), the CDW that splits off the ACC enters the eastern limb of the Weddell gyre, mixes with the cold shelf water, and then forms the Weddell Sea Bottom Water (WSBW), which over time moves upward to replenish the overlying WSDW. The relatively warm and salty WSDW is displaced upward by Ekman pumping due to the negative wind stress curl over the SO and subsequently mixed with the cold and fresh surface water. These facts indicate that the SO sea ice–ocean system is closely connected to the SH westerlies. Meanwhile, the SAM, the

representative climate mode associated with the SH westerlies, is characterized by swings between the stronger and poleward-shifted westerlies in its positive phase and the weaker and equatorward-shifted westerlies in its negative phase (Gong and Wang 1999; Thompson and Wallace 2000). For clarity, we only consider intensification of the SH westerlies without taking into account their meridional movement.

Since the studies of Toggweiler and Samuels (1993, 1995), the influence of the SH westerlies on the global ocean, for example, the Antarctic Surface Water and the Antarctic Intermediate Water (AAIW; e.g., Oke and England 2004), the North Atlantic Deep Water (NADW; e.g., Rahmstorf and England 1997; Brix and Gerdes 2003), the Atlantic Ocean heat transport (e.g., Lee et al. 2011), and the ACC (e.g., Gnanadesikan and Hallberg 2000), has been extensively studied. In this study we aim to investigate how, at the beginning, the intensification of the SH westerlies acts to generate the Weddell Polynya and open-ocean deep convection and how the SO sea ice–ocean system finds its new steady state afterward. The model used is a sea ice–ocean general circulation model (GCM) coupled to a global atmosphere energy balance model (EBM), in which the SH westerlies are intensified by a factor of 1.2. Detailed descriptions of the model and experimental design are given in the next section. All the processes, from preconditioning of the Weddell Polynya to an occurrence of open-ocean deep convection to the decay of the Weddell Polynya, are described in detail in section 3 along with verification of the model results. The final section provides a summary and conclusions.

2. Model description

a. Model configuration

The main framework of the model is the Modular Ocean Model, version 4 (MOM4), of the Geophysical Fluid Dynamics Laboratory (GFDL), in which the primitive equation ocean model (Griffies et al. 2004) is coupled with a dynamic and thermodynamic sea ice model (Winton 2000). It is also coupled with the two-dimensional global atmosphere EBM (Gerdes et al. 2005) and the land model (LM2; Anderson et al. 2004). All model components are coupled via the GFDL Flexible Modeling System (FMS). The sea ice–ocean model (MOM4) extends from 80°S to 90°N with a tripolar grid (Murray 1996), and its horizontal resolution is 2° in longitude and 0.7°–1° in latitude. In the vertical, it contains 50 levels: 22 upper levels with uniform 10-m thickness and 28 lower levels of gradually increasing thickness to about 400 m at 5500-m depth. The bottom layer follows

the actual topography based on Smith and Sandwell (1997) using satellite data in the region from 72°S to 72°N, the National Oceanic and Atmospheric Administration (NOAA) 5-Minute Gridded Global Relief Data (ETOPO5), and the International Bathymetric Chart of the Arctic Ocean (IBCAO). The EBM extends globally and has T42 horizontal resolution. The present model configurations are similar to those used in Gerdes et al. (2005).

The ocean model has an explicit free surface, employing the K-profile parameterization (KPP) scheme of Large et al. (1994) for simulation of the surface mixed layer. It uses the Gent–McWilliams (GM) scheme (Gent and McWilliams 1990) for parameterizing mesoscale eddy mixing on isopycnal surfaces. The coefficients for vertical mixing vary in the upper layers from $10^{-5} \, \mathrm{m^2 \, s^{-1}}$ in the tropics to $3 \times 10^{-5} \, \mathrm{m^2 \, s^{-1}}$ at high latitudes and increase at depth to $1.2 \times 10^{-4} \, \mathrm{m^2 \, s^{-1}}$ following Bryan and Lewis (1979). The model uses the convective scheme of Rahmstorf (1993) for convective adjustment.

The sea ice model consists of three layers, one snow layer and two sea ice layers, and is run on the same grid as the ocean model. The thermodynamics of sea ice is formulated according to Winton (2000), and the physical description of the sea ice dynamics involves the viscous–plastic constitutive law introduced by Hibler (1979) from rheological principles.

The EBM provides thermodynamic forcing by solving prognostic equations for atmospheric temperature and specific humidity. Atmospheric temperature is determined by the surface heat balance calculation composed of shortwave radiation, longwave radiation, and sensible and latent heat fluxes. The balance between evaporation and both liquid and frozen precipitation determines the specific humidity. It should be noted that the wind field and precipitation are not calculated by the EBM but are directly derived from data. Bulk formulas are used to calculate heat and momentum fluxes at the ocean or sea ice surface. The atmospheric dataset contains monthly-mean wind fields from the 15-yr European Centre for Medium-Range Weather Forecasts (ECMWF) Re-Analysis (ERA-15) data between 1979 and 1993, which is augmented by daily variability from a selected year (1982). The sea ice–ocean model is repeatedly forced by the day-to-day variability of this year.

b. Experimental design

According to reanalyses with phases 3 and 5 of the Coupled Model Intercomparison Project (CMIP) (Swart and Fyfe 2012), the SH westerlies have been significantly intensified over the last 30 years, although its annual-mean jet position did not show a robust trend. The objective of this study is to investigate the response of the
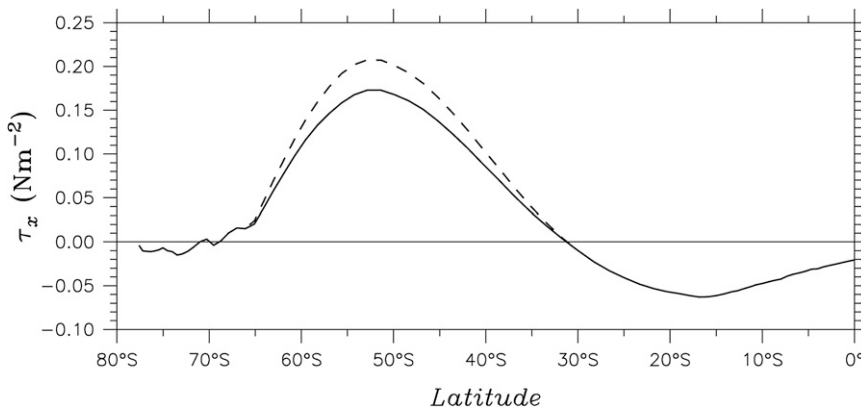
FIG. 2. Zonal-mean zonal wind stress τ_x for CTRL (solid) and SW20 (short dashed lines).

SO sea ice–ocean system to the intensification of the westerlies at the beginning of this interval. Figure 2 shows the zonal-mean zonal wind stress for the control case (hereafter denoted as CTRL) and the intensified SH westerlies (hereafter denoted as SW20), respectively. In CTRL the wind stress is as stated above, while in SW20 only the zonal wind stress in the latitudinal band between 66° and 32°S is uniformly intensified by a factor of 1.2. In the wind field employed in the model, this latitudinal band covers most of the area dominated by the SH westerlies [40-yr ECMWF Re-Analysis

(ERA-40) data between 1957 and 2002] and the ACC (Orsi et al. 1995). In the CTRL experiment, the model starts from a "cold start" condition and is run for 500 years as a spinup period. This is not enough for the whole bottom water mass to reach a full equilibrium state, that is, a variation of global-mean bottom water properties smaller than $0.01°C \, (100 \, yr)^{-1}$ for temperature and $0.001 \, psu \, (100 \, yr)^{-1}$ for salinity (England 1993). However, as discussed in the following section, most main features of the global ocean circulation and the SO sea ice are in a reasonable range and are thus
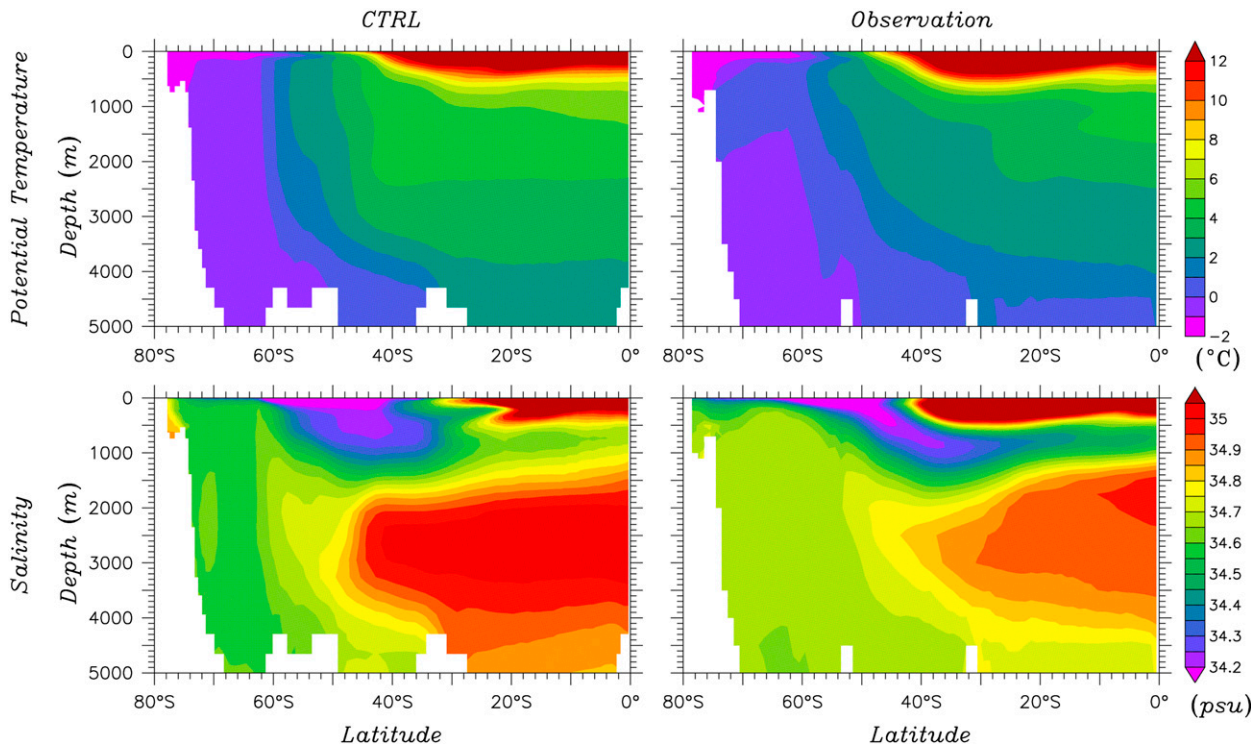

FIG. 3. Zonal-mean potential temperature and salinity in the Atlantic (60°–10°W) for CTRL (20-yr mean over 481 and 500) and observation (Locarnini et al. 2006; Antonov et al. 2006).
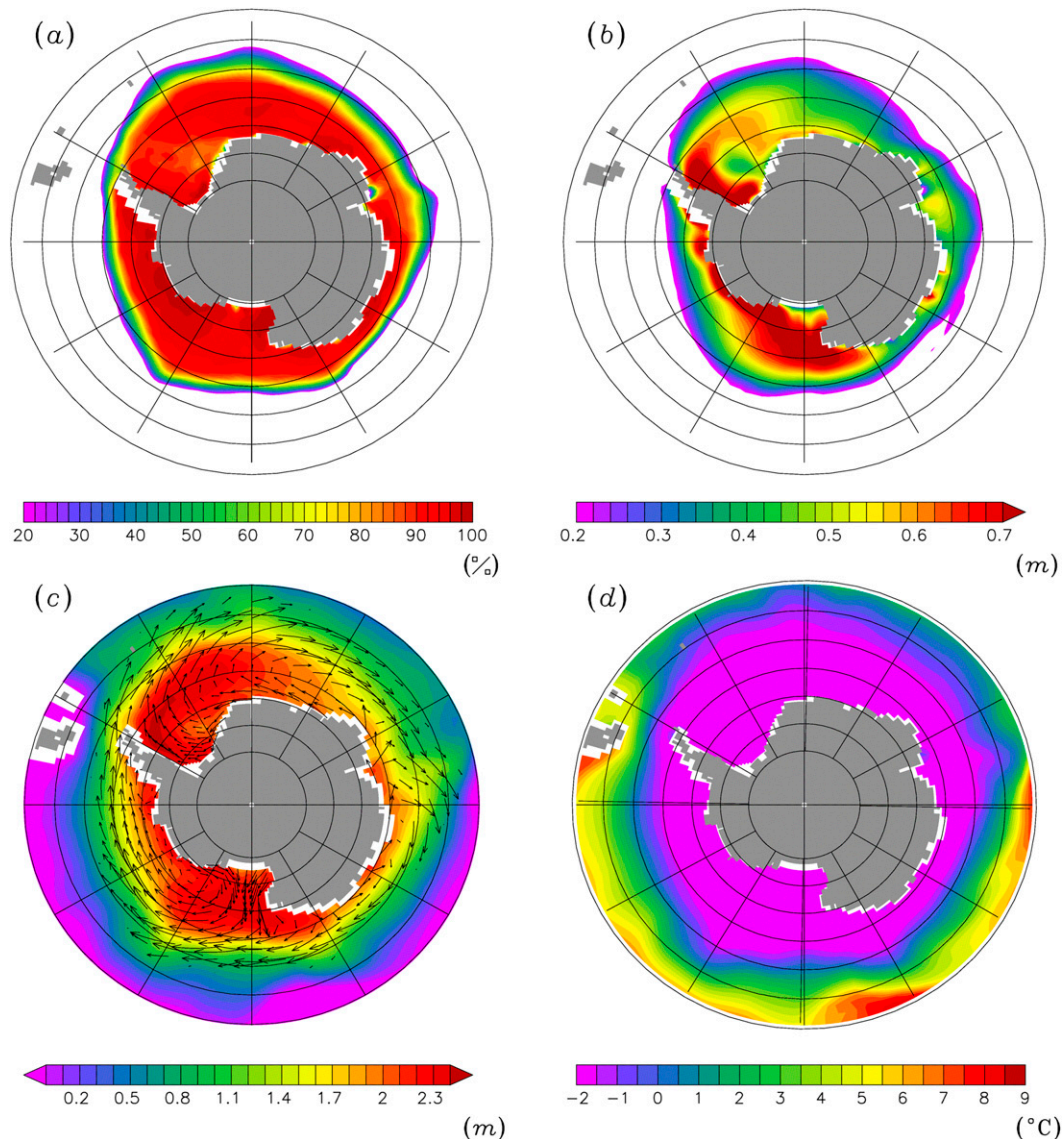
FIG. 4. Horizontal distributions of the winter-mean sea ice (a) concentration, (b) thickness, (c) sea surface height with sea ice drift, and (d) upper-ocean temperature (≥50 m) for CTRL over the period of the last 20 years (481–500). Only the sea ice whose concentration is higher than 20% is presented.

judged to be in a suitable state for this type of sensitivity experiment. After the spinup, the SW20 experiment starts from the last year of CTRL and is run for 100 years. Our analysis is conducted for the whole 100 years of the SW20 experiment. All variables analyzed in this paper are calculated inside of the model.

In this study, the SH westerlies are intensified by only a factor of 1.2, smaller than factors ranging from 1.5 to 3.0 applied in many previous studies (Toggweiler and Samuels 1993, 1995; Rahmstorf and England 1997; De Boer et al. 2008). Although not presented in this paper, an experiment in which the SH westerlies were intensified by a factor of 1.5 was also performed; the response of the SO sea ice–ocean system was more drastic and faster than that with the SH westerlies intensified by a factor of 1.2, but main phenomena such as the Weddell Polynya and open-ocean deep convection occurred via the same process in both experiments. Moreover, because we focus on the transition period when the weakened SH westerlies begin to regain strength, a relatively small increase factor is employed in this study to explore whether the SO sea ice–ocean system is susceptible to a small change in the SH westerlies.
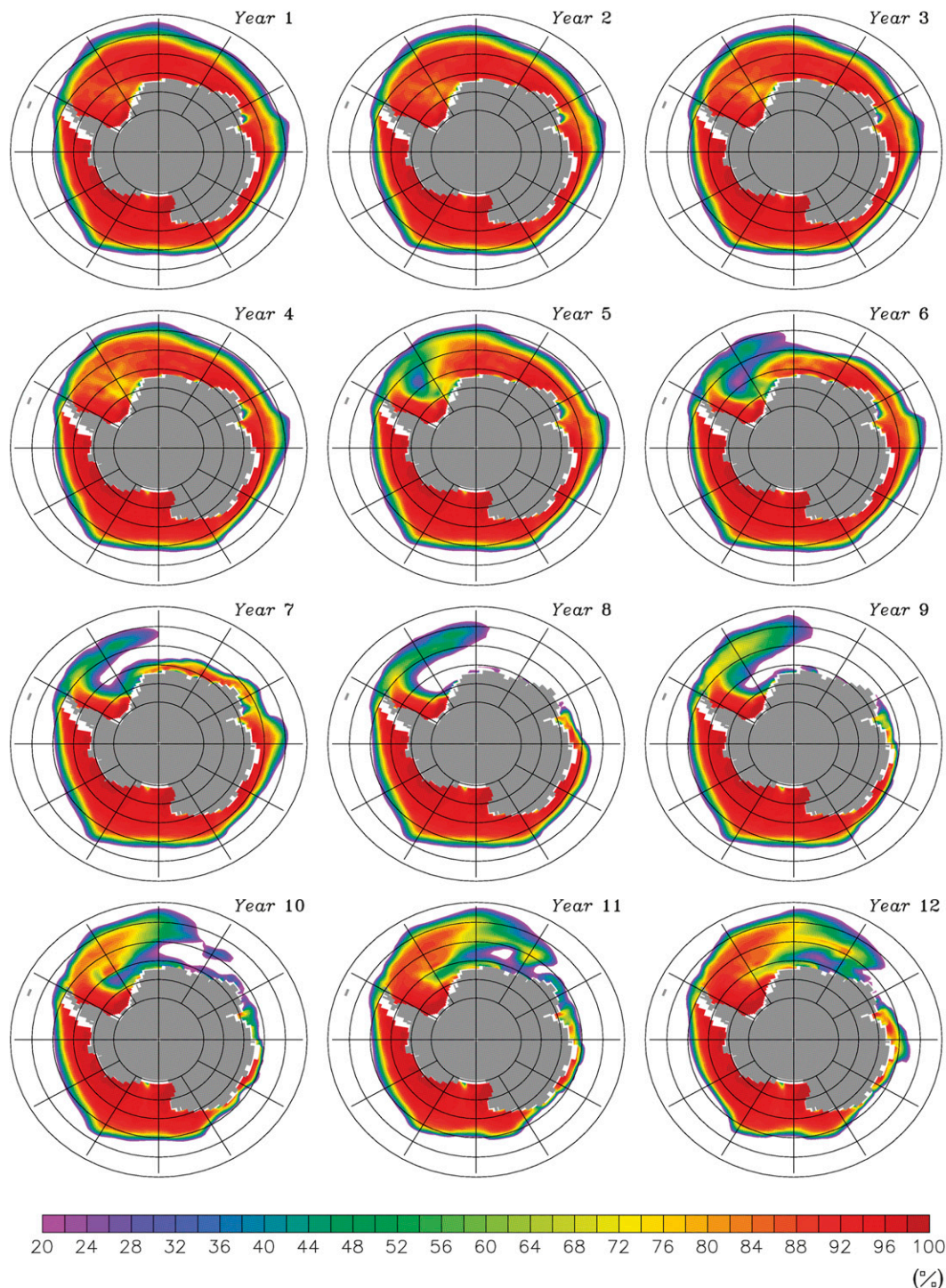
FIG. 5. Horizontal distributions of the winter-mean (June–August) sea ice concentration over the first 24 years of the SW20 integration.

3. Results

a. Control run

Figure 3 shows meridional sections of zonal-mean, annual-mean SH Atlantic potential temperature and salinity for CTRL and observed data (Locarnini et al. 2006; Antonov et al. 2006), respectively. Though differing in magnitude in comparison with the observational data, CTRL indicates a northward intrusion of the AAIW and a southward intrusion of the NADW in its
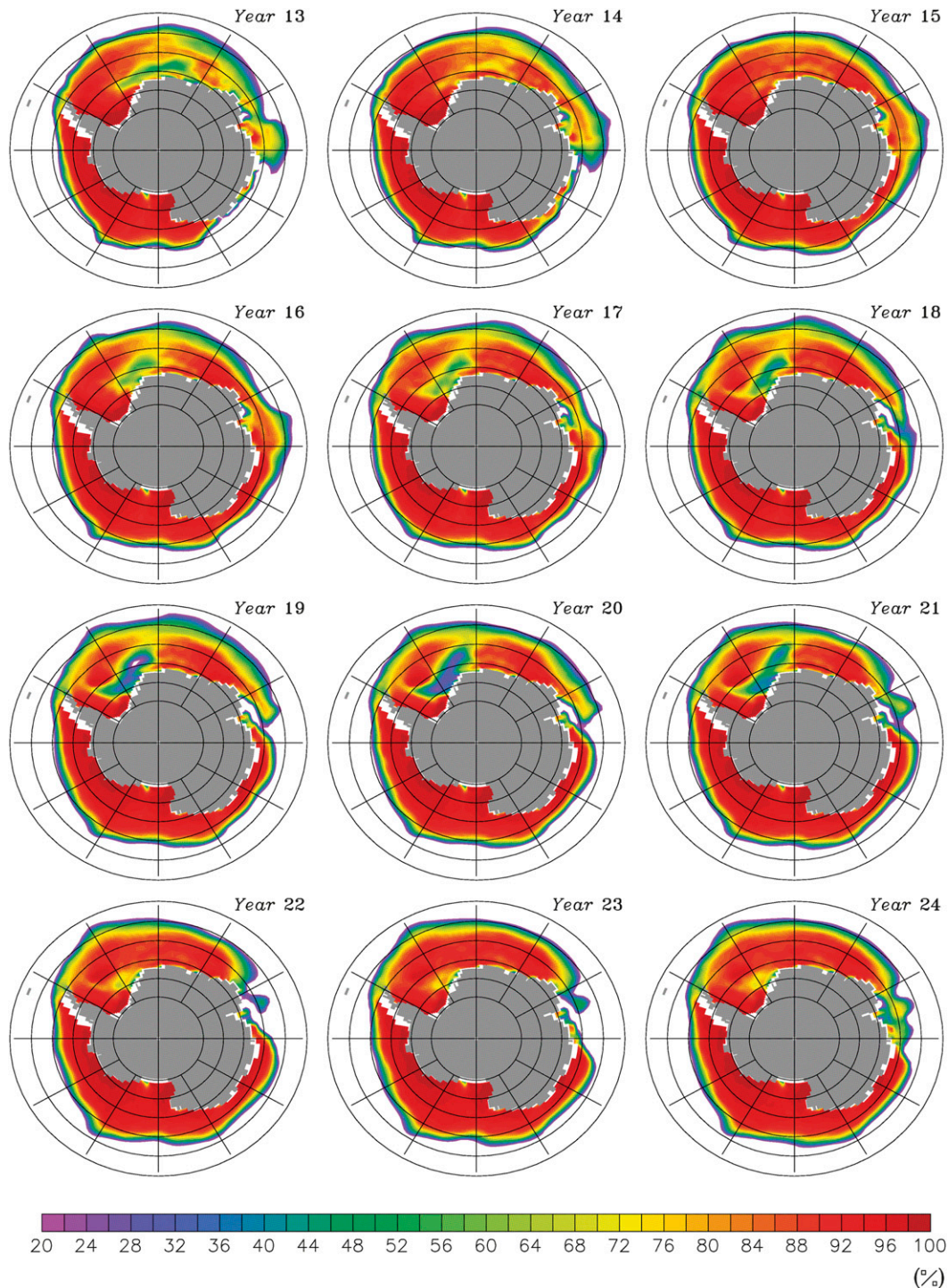
FIG. 5. (*Continued*)

salinity distribution. In the SO to the south of 60°S, however, a tongue of relatively warm deep water cannot be found in CTRL, and the whole water column is fresher than in the observations. The Atlantic meridional overturning circulation (MOC) and the NADW outflow are main choke points of the thermohaline circulation in the Atlantic Ocean and affect the volume transport of the ACC bordering the Weddell gyre via thermal wind balance (McDermott 1996; Gnanadesikan and Hallberg 2000). The Atlantic MOC at 30°N reaches 21.7 Sverdrups
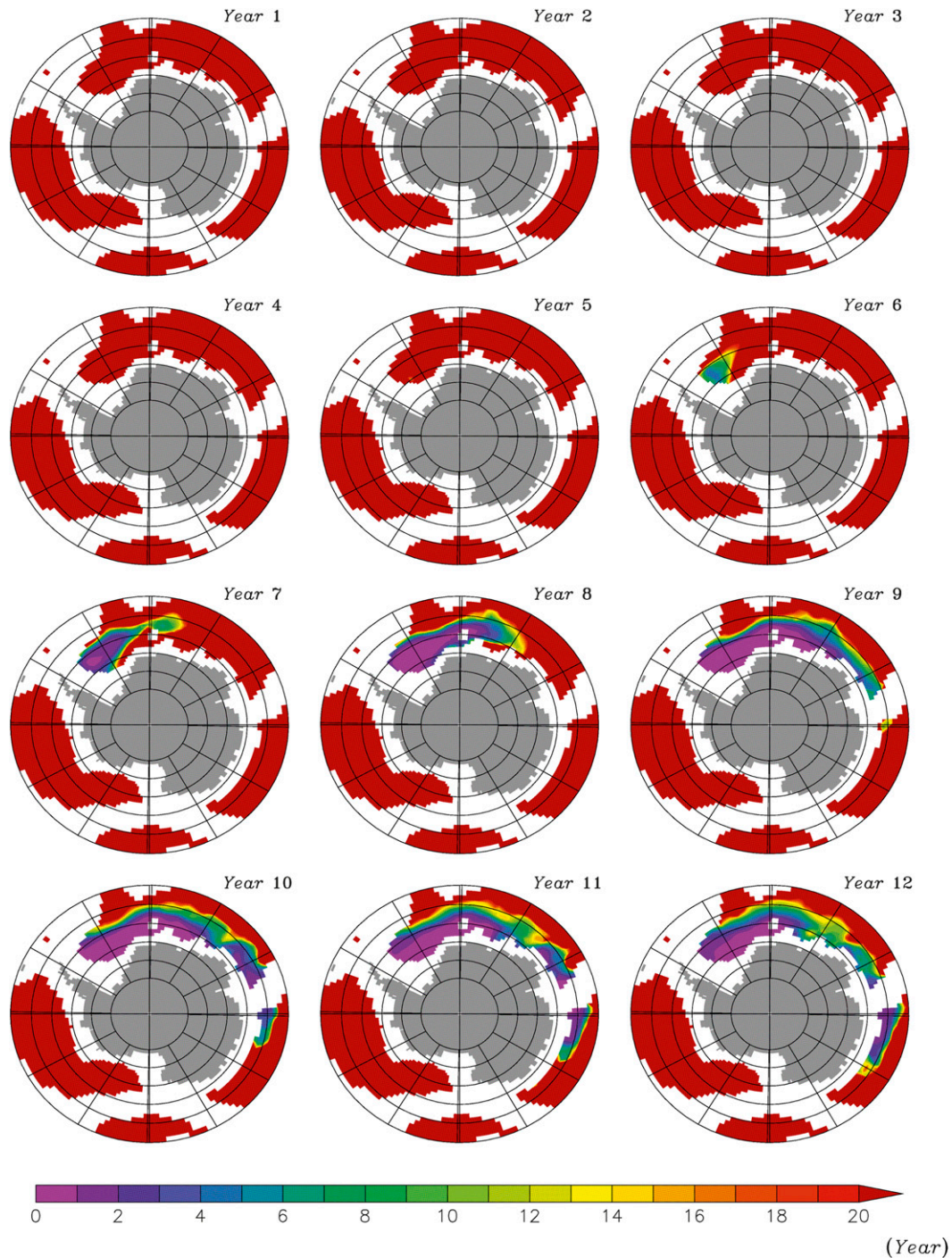
FIG. 6. Horizontal distributions of the annual-mean AOW at 4000-m depth over the first 24 years of the SW20 integration.

(Sv; $1 \, \mathrm{Sv} \equiv 10^6 \, \mathrm{m}^3 \, \mathrm{s}^{-1}$), placing it near the upper bound of values from climate models for the present-day climate [see Fig. 10.15 of Solomon et al. (2007)]. The NADW outflow passing through 30°S is 20.6 Sv and is also larger than the observed estimate [from ~17 to ~18 Sv according

to Ganachaud and Wunsch (2000) and Dong et al. (2009)]. The transport of the ACC across the Drake Passage is 189.1 Sv. This is greater than the observed transports that vary between 110 and 150 Sv (Whitworth et al. 1982; Orsi et al. 1995; Cunningham et al. 2003), but is
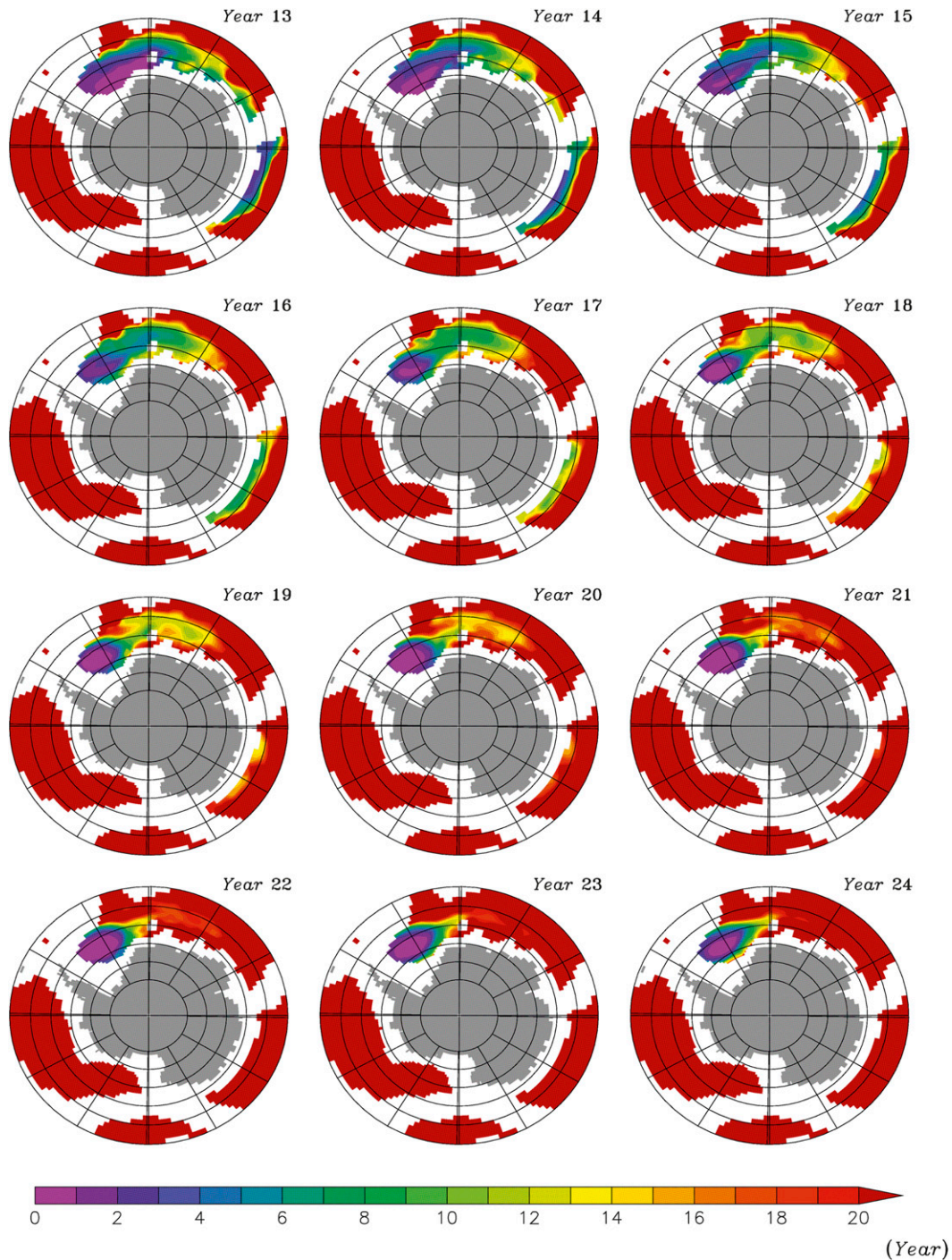
FIG. 6. (*Continued*)

in agreement with other modeling results (Hallberg and Gnanadesikan 2006; Kuhlbrodt et al. 2012). The global-mean potential temperature at 4000-m depth reaches 1.63°C and is higher than the observed estimate [1.08°C according to Levitus (1982)]. These results are attributed to the relatively large Atlantic MOC, which is linked to larger NADW outflow and enhances the ACC via thermal wind balance.

Figures 4a and 4b show the austral winter–mean (June–August) sea ice concentration and thickness surrounding Antarctica over the last 20 years (481–500) of the CTRL integration period. Although performed in the framework

of the coarse-resolution model, they are in overall agreement with results of other ice–ocean coupled models (Fichefet et al. 2003; Stössel 2008) and observations (Maksym and Markus 2008; Parkinson and Comiso 2008). The distribution of the sea ice thickness is similar to that of the winter-mean sea surface height (Fig. 4c): relatively thick (thin) sea ice is observed where the winter-mean sea surface height is relatively low (high). It seems that the southern limb of the Weddell gyre acts to push sea ice westward and thus the sea ice piles up in the western limb of the gyre. Although most pack ice consists of sea ice concentrations higher than 92%, there is a small area in the central Weddell Sea where the sea ice concentration drops to 82% at most. According to satellite observations (Parkinson and Comiso 2008), this region is generally covered by highly concentrated sea ice. Thus, one might argue that our model has a preference for an open-ocean polynya in the central Weddell Sea, but the winter-mean upper-ocean temperature (<50-m depth) uniformly lower than $-1.5°C$ under sea ice cover (Fig. 4d) is important evidence to dispel this concern.

Within the SW20 experiment, the Weddell Polynya could be generated in two ways: a dynamic way due to a wind- and current-driven divergent sea ice drift and a thermodynamic way due to upwelled relatively warm WSDW melting the sea ice. The uniformly near-freezing upper-ocean temperature under sea ice cover in CTRL indicates that the relatively less concentrated and thinner sea ice in the central Weddell Sea is not due to surface warming but to sea ice drift. As discussed in detail in the following section, the simulated Weddell Polynya is due to the upwelled relatively warm WSDW. These imply that the modeled SO sea ice in CTRL does not have an intrinsic tendency to generate Weddell Polynyas.

In summary, the simulated ocean states are within reasonable ranges, although the global thermohaline circulation does not reach an equilibrium state in terms of criteria suggested by England (1993); that is, the water temperature and salinity at 4000-m depth still increase about 0.02°C and 0.002 psu during the last 100 years of CTRL. The simulated sea ice shows reasonably good agreement with observations. Therefore, the SO sea ice–ocean system simulated in CTRL is appropriate for investigating its responses to SW20.

b. Opening of the Weddell Polynya

Figures 5 and 6 show horizontal distributions of winter-mean sea ice concentration and annual-mean age of water (AOW) at 4000-m depth over the first 24 years of SW20 integration, in which the AOW indicates how old the water masses are after sinking from the surface. Immediately after the SH westerlies are intensified by

a factor of 1.2, sea ice concentration in the vicinity of 68°S, 38°W starts to decrease gradually. At year 5 the sea ice concentration suddenly drops at maximum to 32% (Fig. 5), at year 6 the younger water mass begins to appear at 4000-m depth, and at year 7 the 1-yr-old water mass is observed at depth (Fig. 6). This means that the surface water sinks to this depth in just 2 years after the drastic reduction of sea ice in the central Weddell Sea, which is clear evidence for open-ocean deep convection and is in good agreement with the observed results of Gordon (1982). That is, the water column beneath the ice-reduced area is destabilized by the dense water newly formed by the extreme cooling and the ensuing sea ice formation releasing salt to the ocean, leading to open-ocean deep convection. Figure 7 shows time series of the maximum barotropic streamfunction in the Weddell Sea (i.e., the intensity of Weddell gyre) and the AOW at 1000-m depth over the whole period of SW20 integration. At first both show gradual changes until year 4. The rate of change is slightly larger in year 4 than in year 3. Then at year 5, when the sea ice in the central Weddell Sea is drastically reduced, the Weddell gyre is also drastically intensified and open-ocean deep convection begins to occur, as indicated by the AOW getting younger at 1000-m depth (see the purple line of Fig. 7). In the case of the 1970s Weddell Polynya, the sea ice concentration dropped below 15% (Carsey 1980), whereas in the fifth year of the SW20 simulation it dropped only to 32%. Although afterward the sea ice concentration continued to drop and at year 7 reached below 15%, in this paper the Weddell Polynya is considered to occur first at year 5 because open-ocean deep convection, which is the most important event resulting from the Weddell Polynya, is triggered that year.

The ice-free area expands eastward south of Australia to the South Pacific Ocean and becomes largest in year 8 as can be seen in Fig. 5. The ice reduction outside of the Weddell Sea is not related to the Weddell Polynya, but to the experimental setup, which is explained with the detailed mechanism of Weddell Polynya in the following. At year 9 the ice-free area starts to shrink and disappears completely by year 15 when the SO sea ice is fully recovered. The surface water masses beneath the areas where the sea ice disappears keep sinking to the bottom during this period. At year 16 sea ice again starts to open gradually, but this time it is closer to the coast and just west of the Greenwich meridian, thus closer to the site of the observed 1970s Weddell Polynya and on a much smaller scale than the first one.

The Weddell Polynya occurs again in year 19, disappears in the next year, and never occurs again during the next 76 model years. As shown in Fig. 7, after the first occurrence of Weddell Polynya, the intensity of the Weddell gyre reaches its peak at years 7 and 8, thereafter
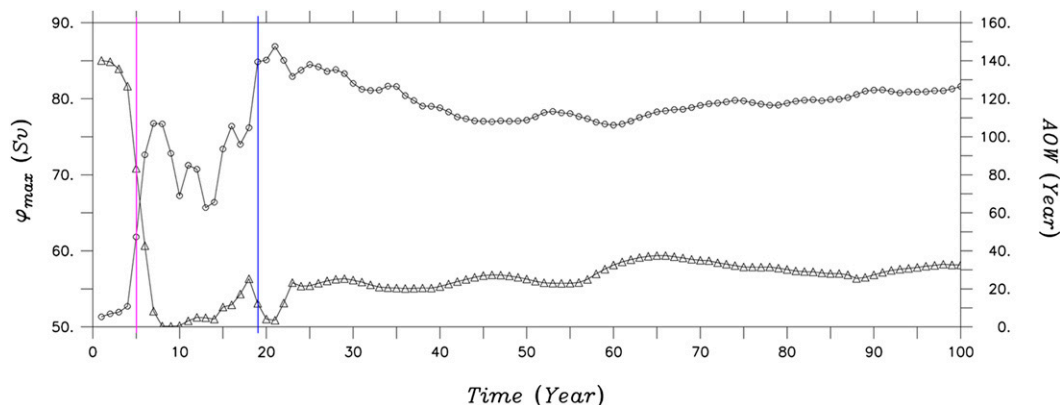
FIG. 7. Time series of the max winter-mean horizontal barotropic streamfunction in the Weddell Sea (black line with circles) and of the winter-mean AOW at 1000-m depth in the central Weddell Sea (black line with triangles). The former is indicative of the intensity of Weddell gyre and is averaged between 80° and 60°S and between 60°W and 20°E, and the latter is averaged between 75° and 65°S and between 40° and 10°W. The purple (blue) line is indicative of the time when the first (second) Weddell Polynya occurs.

oscillates, and shows a sudden increase at year 19. The AOW at 1000-m depth reaches its minimum at years 8, 9, and 10 when open-ocean deep convection is active, gets older from years 11 to 18, indicating that the convection gets weakened, and suddenly gets younger at year 19, indicating that the convection is triggered again. At year 19 the sea ice concentration in the central Weddell Sea also drops below 20%, and thus the second Weddell Polynya is considered to occur at this year.

In the aforementioned small area where the sea ice concentration is originally low, sea ice concentration slightly decreases from 82% to 76% after the second polynya event and maintains this condition to the end of SW20 experiment. It should be noted that, even after the Weddell Polynyas are closed, the narrow chimney lasts until the end of the SW20 experiment (not shown here), which is attributed to the slightly warmed SST in the spot that becomes the cause of additional salt rejection due to sea ice formation [discussed in the next subsection, with Fig. 11 (described in greater detail below)]. We speculate that this salt rejection anomaly—and thus the weakly stratified water column—causes the narrow chimney to remain to the end of the SW20 experiment. When the SH westerlies regain their original state in an additional experiment, this narrow chimney disappears in a few years (not shown here).

c. Detailed mechanism to trigger open-ocean polynya and deep convection

How does the application of SW20 trigger an open-ocean polynya and deep convection in the Weddell Sea? The sea ice–ocean interactions when the first Weddell Polynya starts to form are examined from various angles in the following. Figure 8 shows changes in the winter-mean

SST and AOW at the second layer over the first 6 years of the SW20 integration when the Weddell Polynya first occurs. The second layer's AOW is selected because the first layer is always turned into new water (i.e., zero-age water). The new water, shaded by purple color, is indicative of sinking down from the surface, while the older water shaded by other colors is indicative of the upwelling of deep water. After the SH westerlies are intensified, SST in the central Weddell Sea rises very slowly until year 3, begins to show an obvious increase at year 4, and reaches at most −0.9°C at year 5, which is consistent with the location and period where the first Weddell Polynya appears. Changes in the SST are very similar to changes in the second layer's AOW, which indicate a strong upwelling of deep water at year 4. This confirms that the surface warming in the Weddell Sea is attributed to the upwelling of the relatively warm WSDW. Note that upwelled warm deep waters are older than the surrounding ones at the observed depth. Meanwhile, the aforementioned ice-reduced area outside of the Weddell Sea is also attributed to the relatively warm deep water upwelled at the location, which is associated with the experimental setup that intensifies the zonal wind uniformly between 66° and 32°S and thus gives rise to upwelling of deep water outside of the Weddell Sea.

Figure 9 shows a detailed representation of this upwelling with zonal-mean, winter-mean potential temperature, and zonally integrated, winter-mean meridional streamfunction between 45° and 30°W where the first polynya occurs. In CTRL one sees the coldest layer above a black dotted line (≤−1.2°C), preventing the relatively warm WSDW from entraining into the mixed layer. With the application of SW20, the enhanced wind stress curl over the SO intensifies not only upwelling of the CDW
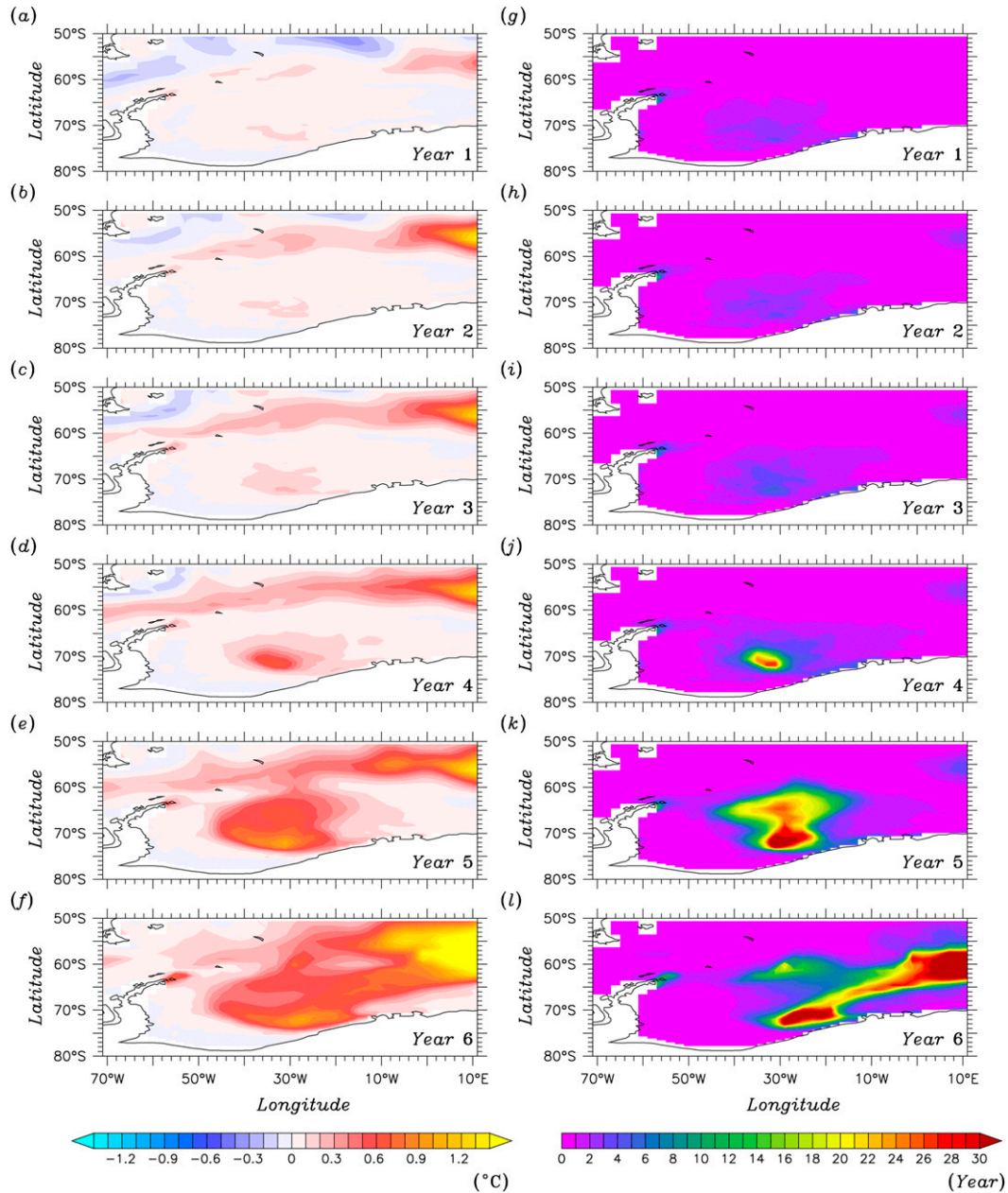
FIG. 8. Changes in the winter-mean (a)–(f) sea surface temperature and (g)–(l) AOW at the second model layer (15-m depth) over the first 6 years of the SW20 integration when the open-ocean polynya event occurs in the Weddell Sea. Note that the AOW in the second layer is shown because it is always set to 0 in the first layer.

but also the Weddell gyre. Although upwelling at year 1 appears to be weaker than that averaged over the last 20 years of CTRL (see Figs. 9a and 9b), it is stronger than that at the last year of CTRL (not shown here), implying that upwelling begins to intensify simultaneously with the application of SW20. As discussed with Fig. 7 above, the Weddell gyre is, regardless of northward Ekman transport outside of it, gradually intensified until year 4 and is drastically intensified at year 5, as illustrated in

Figs. 10a–f. Likewise, in the vicinity of 70°S the upward motion of the WSDW shows gradual change until year 4 and so does the thickness of the coldest layer (see Fig. 9). The rates of change in the upward motion and the thickness of the coldest layer at year 4 are larger than those by year 3. Then at year 5 the upward motion is drastically intensified, and thus the upwelled WSDW destroys the coldest layer completely. This whole thermodynamic process is in a good agreement with the
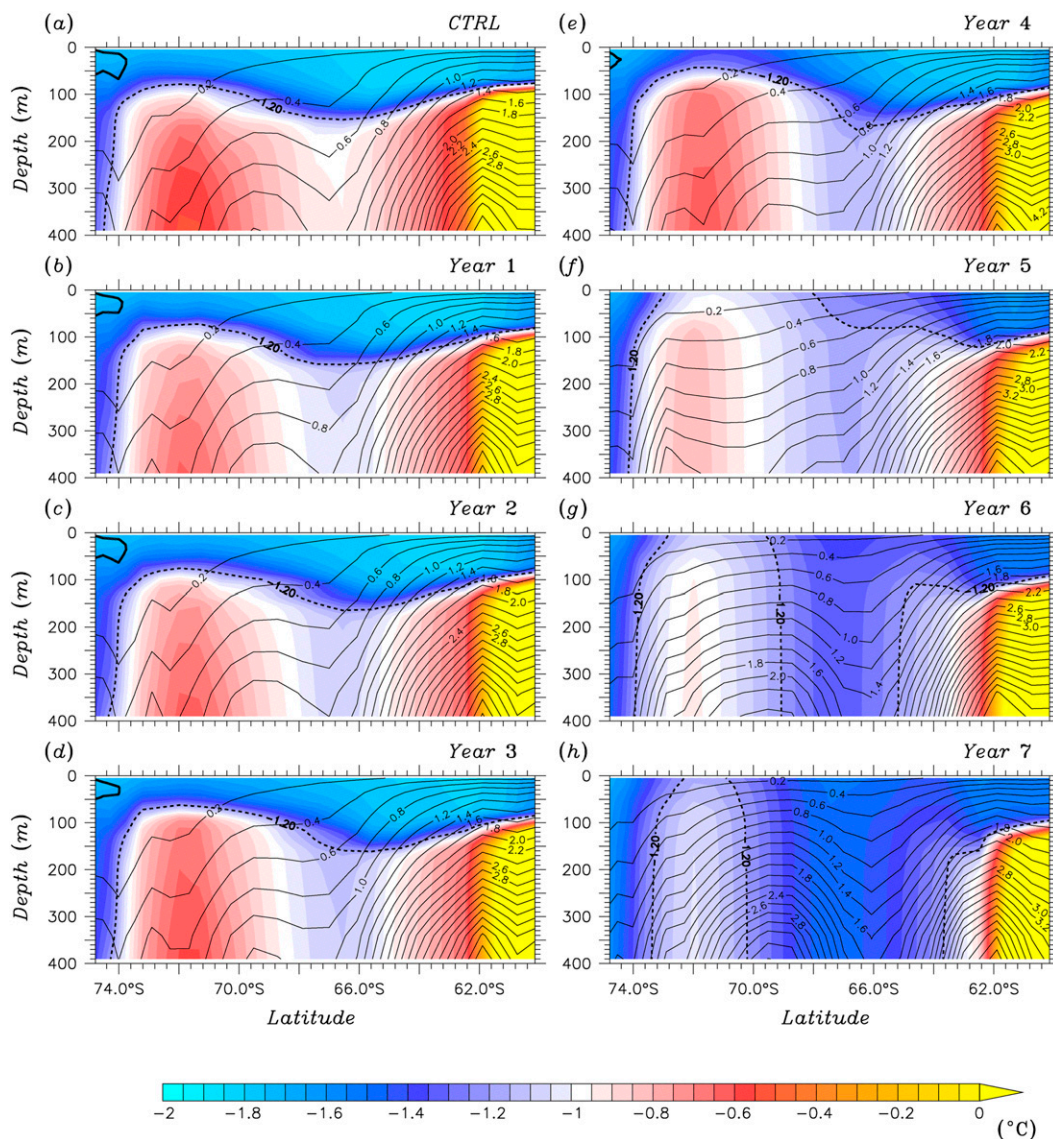
FIG. 9. Meridional sections of zonal-mean, winter-mean potential temperature (color shading), and zonally integrated winter-mean meridional overturning (contours) between 45° and 30°W for CTRL and the first 6 years of the SW20 integration. Positive lines are indicative of clockwise circulation, and their units are Sv. The black dotted line is indicative of the isotherm of −1.2°C.

theory suggested by previous studies (Martinson et al. 1981; Gordon 1982; Gordon and Huber 1984; Martin et al. 2012). Note that the upward motion is dominant in the narrow longitudinal range between 45° and 30°W, but in other areas of the Weddell Sea the downward motion due to near-boundary convection generally prevails and is gradually intensified with the application of SW20 (not shown here). Meanwhile, from years 1 to 4 the cold surface water gradually sinks down near 67°S, and its sinking becomes intense from year 5 in association with open-ocean deep convection, which is consistent with the inference from the AOW at 1000-m depth in

Fig. 7. Moreover, from year 6 the downward motion in the vicinity of 66°S is so intense that the area where the upward motion prevails is pushed poleward and thus becomes small. That is, the Weddell Polynya is generated by the upwelling of warm deep waters, which is, however, suppressed by the ensuing event of open-ocean deep convection. In summary, by year 4 the upward motion is mainly due to the Weddell gyre, at year 5 is drastically intensified by the density overturning triggered by the Weddell Polynya, and from year 6 begins to be rather suppressed by the intense open-ocean deep convection.
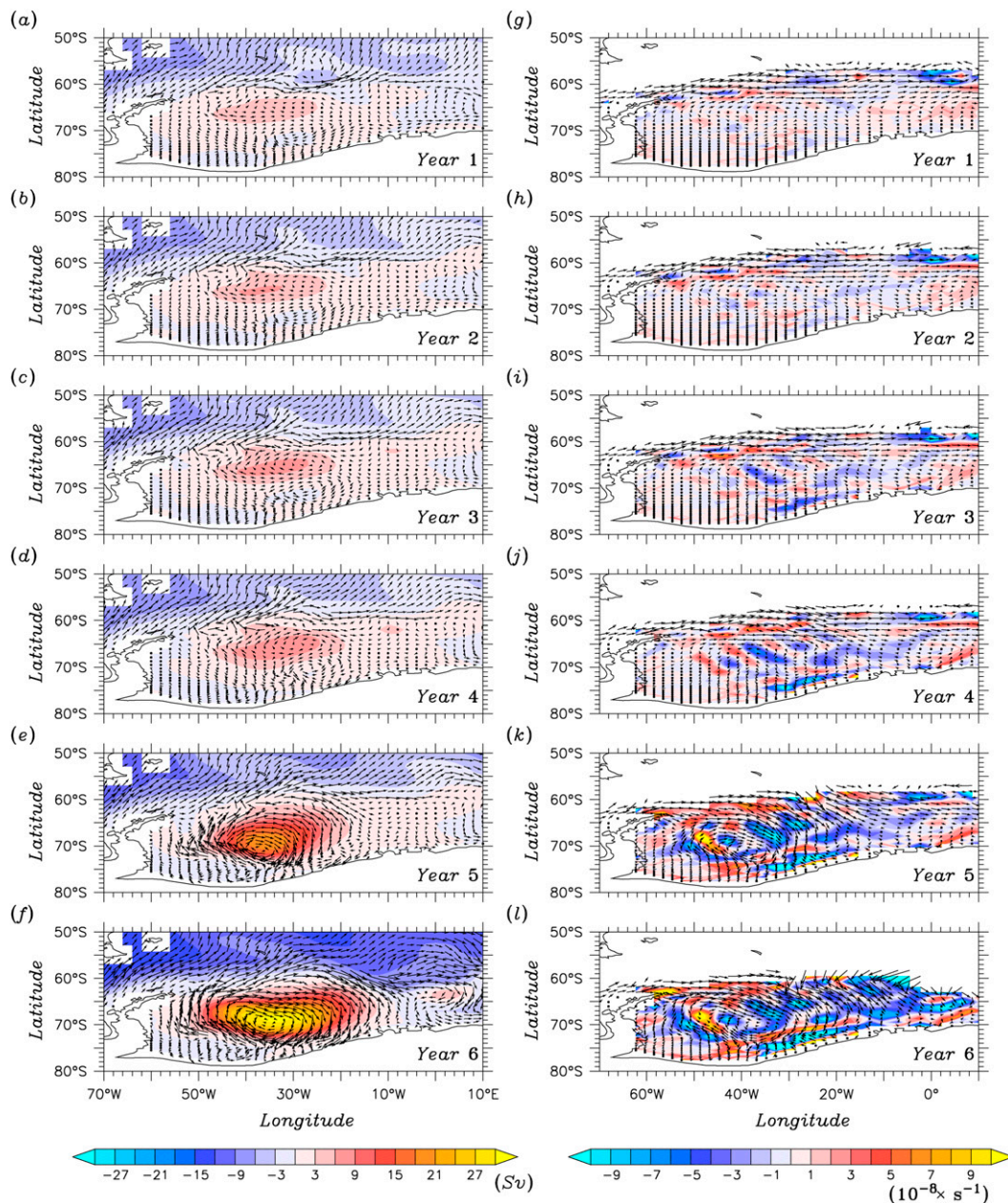
FIG. 10. Changes in (a)–(f) winter-mean horizontal barotropic streamfunction and surface current and (g)–(l) winter-mean sea ice drift and its divergence over the same time period as Fig. 8. A positive (negative) value in the sea ice divergence is indicative of a divergent (convergent) flow.

The next issue is the possibility that the dynamic process associated with the wind- and current-driven divergent sea ice drift plays a role in generating preconditions for the Weddell Polynya. As shown in Figs. 10a–f, immediately after the SH westerlies are intensified, surface water north of 66°S is strongly advected northward by Ekman transport, and more importantly the cyclonic Weddell gyre begins to intensify gradually. While the northward Ekman transport between 60° and 50°S

maintains its increase at year 1 until year 6, the Weddell gyre is, as previously discussed, drastically intensified at year 5 and reaches its peak at years 7 and 8 (see Fig. 7) along with baroclinic intensification of the ACC. These oceanic changes lead to the anomalous cyclonic drift of sea ice but not to its uniform divergence (Figs. 10g–l). This indicates that the simulated Weddell Polynya is not triggered by ocean-to-ice momentum stress from the cyclonic gyre anomaly.
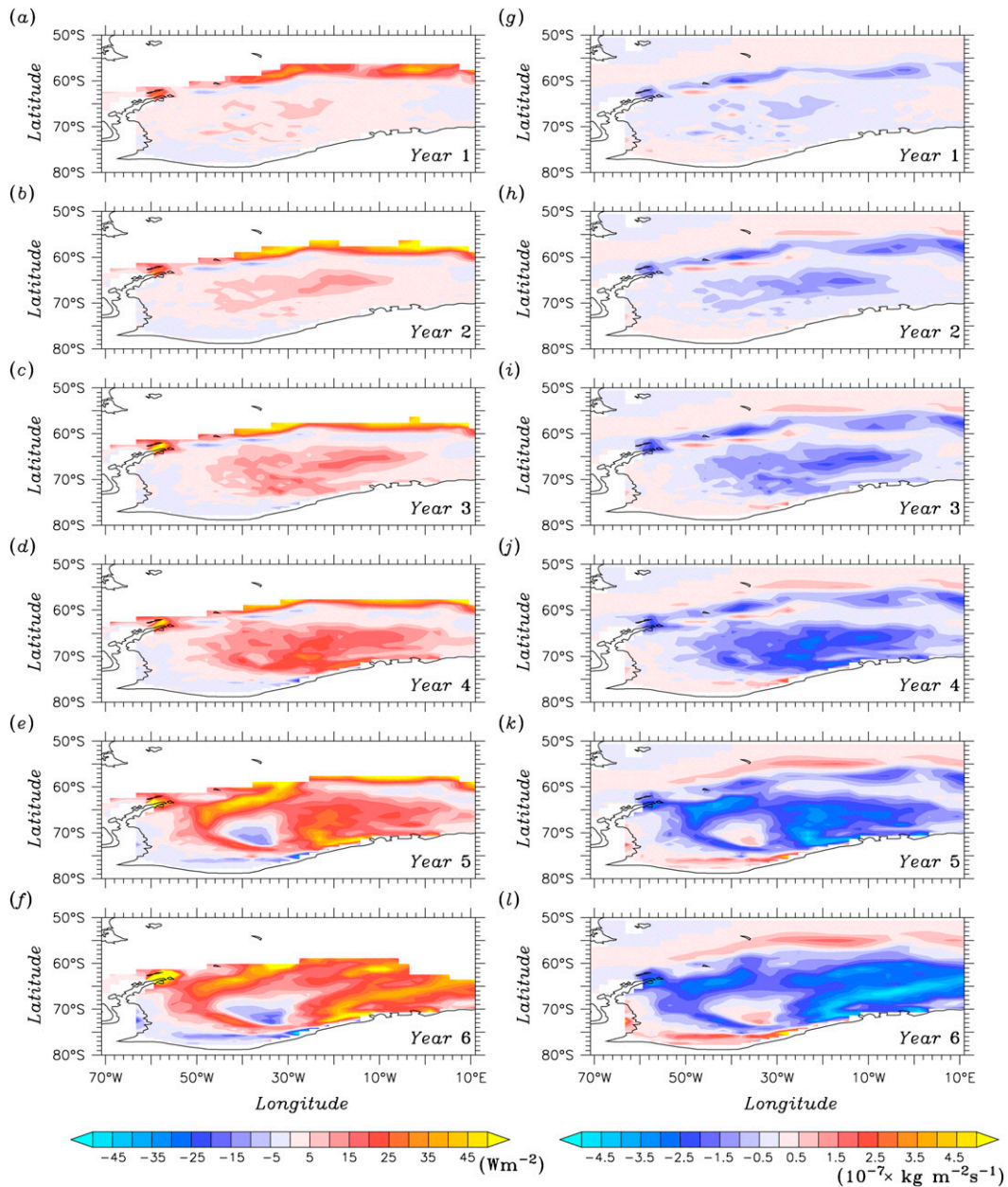
FIG. 11. Changes in the winter-mean (a)–(f) sea ice bottom surface melting energy and (g)–(l) ice–ocean salt flux over the same time period as Fig. 8.

Figure 11 shows changes in the winter-mean sea ice bottom surface melting energy and ice–ocean salt flux for the same initial 6 years of SW20, whose patterns are pretty similar. The upwelled relatively warm water plays a role in melting sea ice (Figs. 11a–d) and preventing sea ice formation, leading to increasingly negative ice–ocean salt flux from the first to fourth winter periods of SW20. Shortly thereafter, relatively warm surface water is exposed to extremely cold air through the Weddell Polynya, which leads to sea ice formation and a corresponding

increase in salt release to the ocean (Figs. 11k and 11l). Sea ice bottom melting energy is thus reduced in the region during this period (Figs. 11e and 11f). These results confirm that surface warming due to upwelling of the WSDW plays a major role in triggering the open-ocean polynya. There are increases in the ice–ocean salt flux along the Weddell Sea coastline (Figs. 10i–l) that are due to an increase in the formation of coastal polynyas. While coastal polynyas are in general controlled by local offshore katabatic winds that push newly formed
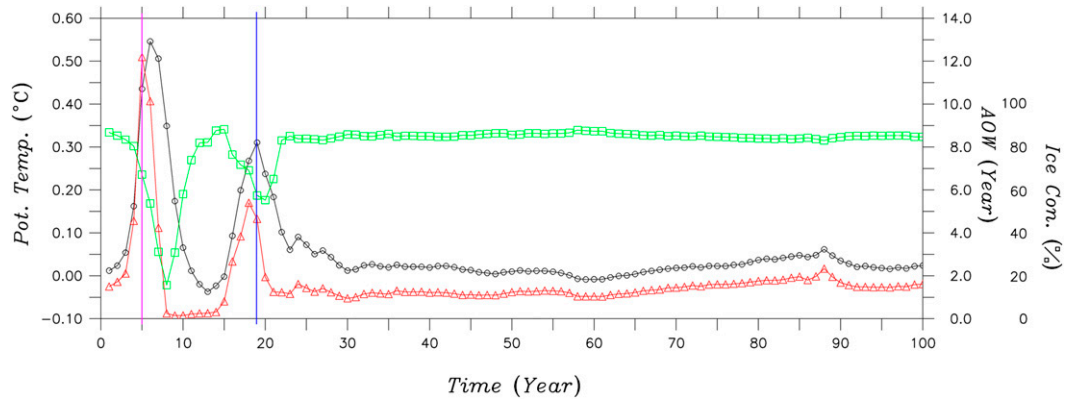
FIG. 12. Time series of winter-mean sea surface temperature anomaly (black line with circle), AOW at the second layer (red line with triangle), and sea ice concentration (green line with square), averaged between 75° and 65°S and between 40° and 10°W, during the whole period of the SW20 integration. The purple (blue) line is indicative of the time when the first (second) Weddell Polynya occurs.

sea ice constantly away from the coastline, in this experiment the offshore sea ice drift anomalies play a role, though they are much weaker than the sea ice drift anomalies in the central Weddell Sea. Although important in increasing dense water formation and thus to enhancing near-boundary convection, these events are not the focus of our study.

d. Differences between the first and second polynya

Together with Fig. 7, sea ice–ocean interactions occurring in the Weddell Sea for the whole integration period of SW20 are summarized in Fig. 12, showing the time series of the areal-mean, winter-mean SST, AOW at the second layer (15-m depth), and sea ice concentration in the region where the simulated Weddell Polynyas occur, and in Fig. 13, showing vertical profiles of winter-mean potential temperature and salinity averaged over the same area for selected years. The processes associated with the first-occurring Weddell Polynya are those described above: 1) cold water at the surface layer is replaced with relatively warm water from the deeper layer via upwelling enhanced by SW20, 2) surface water under the sea ice becomes warm enough to melt sea ice or to prevent its new formation, and 3) sea ice concentration suddenly drops, generating the Weddell Polynya and triggering oceanic deep convection. The surface water becomes warmer in association with the entrained warm deep water and becomes saltier in association with the increased new sea ice formation, while the deep water becomes colder and fresher because the relatively warm and salty deep water masses are mixed with the cold and fresh surface water masses, eventually enhancing instability of the whole water column.

The second-occurring Weddell Polynya is, as illustrated in Figs. 5 and 12, much smaller and persists shorter

than the first polynya. The intensity of upwelling is also much smaller than before and so is the SST increase rate. The processes associated with the second event are slightly different from those of the first event described above. The upwelling ceases between years 8 and 10, gets its strength back very gradually by year 14, in earnest restarts from year 15, and reaches its second peak at year 18. As previously discussed with Fig. 9, for the first Weddell Polynya upwelling is gradually intensified until year 4 along with the Weddell gyre beginning to spin up, reaches its peak at year 5 when the open-ocean polynya triggers the oceanic deep convection, and begins to get weakened from year 6 with the intensification of convection. Similar processes operate for the generation of the second Weddell Polynya. The Weddell gyre weakens between years 8 and 10, oscillates until year 14, and begins to be intensified from year 15 (see Fig. 7). Between years 15 and 18, surface water sinking is weakened (black line with triangles in Fig. 7), and the upwelling starts to recover its strength (red line with triangles in Fig. 12). As indicated by comparison between vertical profiles of potential temperature in years 14 and 18 in Fig. 13, during this period the surface water again becomes warmer because of recovered upwelling, and the deep water also becomes warmer because of reduced sinking of cold surface water. At year 19, which is 1 year after the upwelling reaches its second peak, the gyre shows a substantial spinup (black line with circles in Fig. 7) and the SST in the central Weddell Sea reaches its second peak (black line with circles in Fig. 12), triggering the second polynya near 68°S, 15°W (Fig. 5 and green line with squares in Fig. 12). Consequently, the convection regains its strength (black line with triangles in Fig. 7) and begins to suppress the upwelling (red line with triangles in Fig. 12). In comparison with the first event, the deep
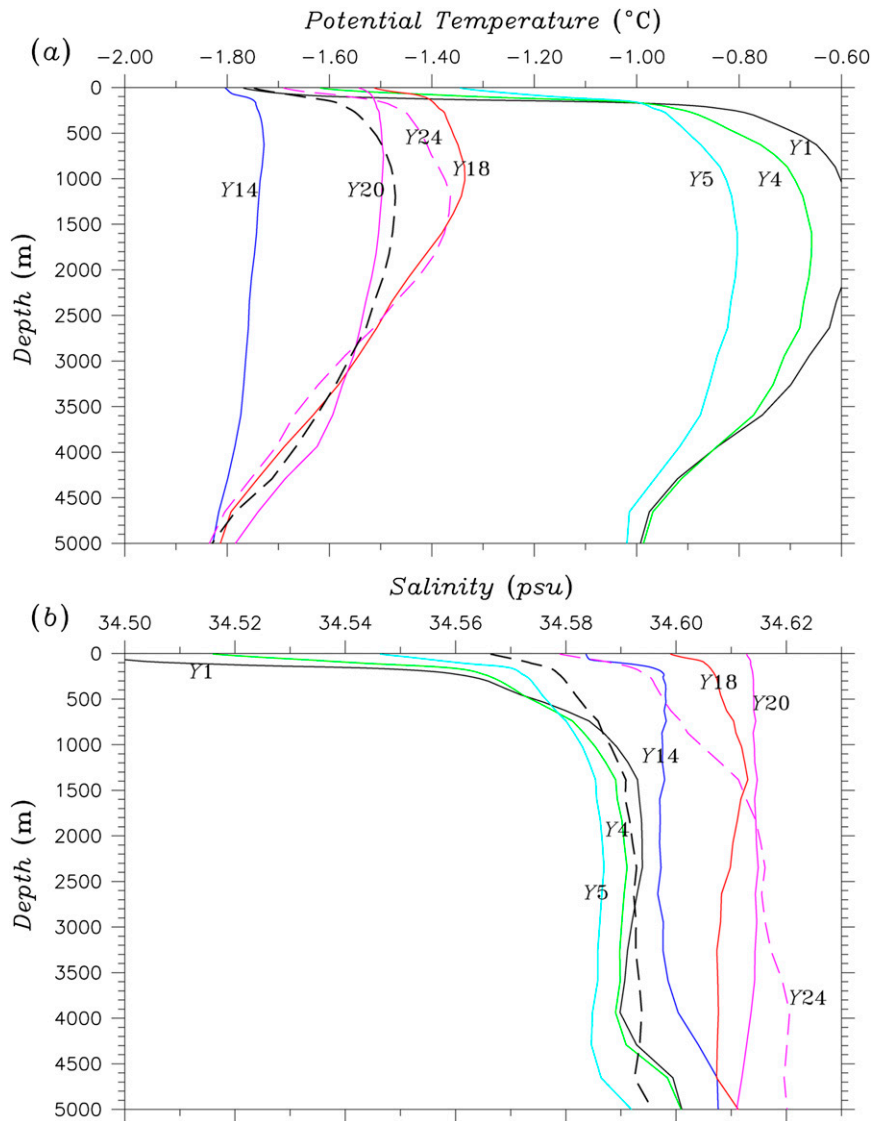
FIG. 13. Vertical profiles of winter-mean (a) potential temperature and (b) salinity, averaged between 75° and 65°S and between 40° and 10°W for the designated years. The black dashed lines are indicative of those averaged over years 81–100 of the SW20 simulation.

water is much colder [see the vertical profile of potential temperature in year 14 (Fig. 13) just before the second upwelling in earnest restarts] because extremely cold surface water keeps sinking to the bottom via open-ocean deep convection until this time. This explains why the second peak of SST is smaller than the first and why the second-occurring Weddell Polynya is much smaller and persists shorter than the first. At year 22, the second polynya is entirely closed (Fig. 5), leading to weakening of open-ocean deep convection (Fig. 7).

Vertical profiles of potential temperature in years 14, 18, 20, and 24 (Fig. 13) reveal an oscillatory mode associated with open-ocean polynya formation and decay,

which is in line with the study of Goosse and Fichefet (2001). Although this oscillatory mode significantly decreases in magnitude after the second Weddell Polynya event ceases, it weakly continues until about year 70 of SW20 (not shown here). The vertical profile of salinity reveals a similar pattern too. At the end of the SW20 model integration, the WSDW reaches its equilibrium state (black dashed lines in Fig. 13).

4. Summary and conclusions

A small step up in the intensity of SH westerlies produces a realistic simulation of the Weddell Polynya

observed between 1974 and 1976. During the first quarter of the 100-yr SW20 simulation, a polynya occurs twice in the central Weddell Sea, leading to open-ocean deep convection, while during the remaining period it never occurs again. Intensification of the SH westerlies increases not only upwelling of CDW but also the Weddell gyre, causing relatively warm WSDW to rise up to the surface in the central Weddell Sea. This appears to play a crucial role in triggering these open-ocean polynya and convection events. The two Weddell Polynya events occur in slightly different locations: the first in the vicinity of 68°S, 38°W, which is slightly southwest of the observed polynya during the 1970s, and the second near the observed one. The second Weddell Polynya is smaller and persists for less time than the first one because upwelling is weaker and the underlying WSDW is colder than when the first occurs.

As discussed in section 3, the relatively low sea ice concentration in the simulated central Weddell Sea does not have a significant influence on the discussion hitherto because the simulated open-ocean polynyas are triggered mainly by thermodynamic processes associated with surface warming that affects sea ice regardless of its concentration and thickness, not by dynamics associated with anomalous divergent drift of sea ice that mainly affects less concentrated and thin sea ice. We expect the result would be unchanged even if the simulated sea ice in the central Weddell Sea was highly concentrated and thick. What determines the location where an open-ocean polynya occurs is dependent on the location where the WSDW mass rises up to the surface, which in turn depends on the inherent capability of the ocean GCM used in the study, such as how accurately the Weddell gyre is reproduced and how well the bottom topography is resolved. Moreover, in order to reproduce the 1970s Weddell Polynya by use of the model, we should consider how much the effective atmosphere–ocean salt flux increases during the prolonged negative phase of the SAM and how the SO winds actually change at the period. The role of Maud Rise also helps focus the polynya location (Ou 1991; Alverson and Owens 1996; Holland 2001).

Even in a relatively short integration time, major ocean flows in the SO reveal their trends clearly. SO overturning is intensified in association with convection events occurring in the SO, leading to an increase in Antarctic Bottom Water (AABW) formation, and Deacon overturning is significantly intensified in association with the enhanced northward Ekman transport below the SH westerlies. Because of the activated SO sea ice–ocean interactions, deep water to the south of the ACC becomes much denser than that to the north of the ACC (not shown here), significantly increasing the Drake Passage Throughflow, that is, the volume transport of ACC, by about 20% to 223.7 Sv in the latter half of the SW20 experiment. When open-ocean polynyas exist and open-ocean convection is most pronounced, the strength of the ACC reaches a maximum of 245.5 Sv. Because the 100-yr integration time of SW20 is too short to evaluate changes associated with the Atlantic MOC, we do not discuss it in this study.

The slight intensification of SH westerlies in the SW20 experiment appeared to play a critical role in triggering the Weddell Polynya and open-ocean deep convection. It should be accompanied by the Weddell Sea adjusting to the relatively weak SH westerlies during the prolonged negative phase of the SAM between 1954 and 1974. As previously discussed in connection with Fig. 1, the effective atmosphere–ocean salt flux due to drier-than-normal atmospheric conditions, proposed by Gordon et al. (2007), will also play an important role in generating preconditions for Weddell Polynyas during the prolonged negative SAM period. The results of SW20 discussed in this study not only satisfy the hypothesis of Gordon et al. (2007) but also provide another clue explaining why a persisting Weddell Polynya has not occurred since the 1970s: there has not been a period to satisfy the prolonged negative phase of SAM followed by a sharp increase in SH westerlies since that time. The long-term response of the global ocean circulation to SW20 will be investigated in detail in a future paper. Moreover, further studies are necessary to assess the response of the SO sea ice–ocean system to a more realistic change in the SH westerlies, for example, SH westerlies gradually oscillating between strengthening and weakening and between pole- and equatorward shifts or to actual wind stress data from a data assimilation model.

REFERENCES

Alverson, K., and W. B. Owens, 1996: Topographic preconditioning of open-ocean deep convection. *J. Phys. Oceanogr.,* **26,** 2196–2213.

Anderson, J. L., and Coauthors, 2004: The new GFDL global atmosphere and land model AM2–LM2: Evaluation with prescribed SST simulations. *J. Climate,* **17,** 4641–4673.

Antonov, J. I., R. A. Locarnini, T. P. Boyer, A. V. Mishonov, and H. E. Garcia, 2006: *Salinity.* Vol. 2, *World Ocean Atlas 2005,* NOAA Atlas NESDIS 62, 182 pp.

Brix, H., and R. Gerdes, 2003: North Atlantic Deep Water and Antarctic Bottom Water: Their interaction and influence on the variability of the global ocean circulation. *J. Geophys. Res.,* **108,** 3022, doi:10.1029/2002JC001335.

Bryan, K., and L. J. Lewis, 1979: A water mass model of the world ocean. *J. Geophys. Res.,* **84** (C5), 2503–2517.

Cai, W., and P. Baines, 1996: Interactions between thermohaline- and wind-driven circulations and their relevance to the dynamics of the Antarctic Circumpolar Current, in a coarse-resolution global ocean circulation model. *J. Geophys. Res.,* **101** (C6), 14 073–14 093.

Carsey, F. D., 1980: Microwave observations of the Weddell Polynya. *Mon. Wea. Rev.,* **108,** 2032–2044.

Cunningham, S. A., S. G. Alderson, B. A. King, and M. A. Brandon, 2003: Transport and variability of the Antarctic Circumpolar Current in Drake Passage. *J. Geophys. Res.,* **108,** 8084, doi:10.1029/2001JC001147.

De Boer, A. M., J. R. Toggweiler, and D. M. Sigman, 2008: Atlantic dominance of the meridional overturning circulation. *J. Phys. Oceanogr.,* **38,** 435–450.

Dong, S., S. L. Garzoli, M. O. Baringer, C. S. Meinen, and G. J. Goni, 2009: Interannual variations in the Atlantic meridional overturning circulation and its relationship with the net northward heat transport in the South Atlantic. *Geophys. Res. Lett.,* **36,** L20606, doi:10.1029/2009GL039356.

England, M. H., 1993: Representing the global-scale water masses in ocean general circulation models. *J. Phys. Oceanogr.,* **23,** 1523–1552.

Fichefet, T., B. Tartinville, and H. Goose, 2003: Antarctic sea ice variability during 1958–1999: A simulation with a global ice–ocean model. *J. Geophys. Res.,* **108,** 3102, doi:10.1029/2001JC001148.

Ganachaud, A., and C. Wunsch, 2000: Improved estimates of global ocean circulation, heat transport and mixing from hydrographic data. *Nature,* **408,** 453–457.

Gent, P. R., and J. C. McWilliams, 1990: Isopycnal mixing in ocean circulation models. *J. Phys. Oceanogr.,* **20,** 150–155.

——, W. G. Large, and F. O. Bryan, 2001: What sets the mean transport through Drake Passage? *J. Geophys. Res.,* **106** (C2), 2693–2712.

Gerdes, R., W. Hurlin, and S. M. Griffies, 2005: Sensitivity of a global ocean model to increased run-off from Greenland. *Ocean Modell.,* **12,** 416–435.

Gnanadesikan, A., and R. W. Hallberg, 2000: On the relationship of the circumpolar current to Southern Hemisphere winds in coarse-resolution models. *J. Phys. Oceanogr.,* **30,** 2013–2034.

Gong, D., and S. Wang, 1999: Definition of Antarctic Oscillation index. *Geophys. Res. Lett.,* **26,** 459–462.

Goosse, H., and T. Fichefet, 2001: Open-ocean convection and polynya formation in a large-scale ice–ocean model. *Tellus,* **53A,** 94–111.

Gordon, A. L., 1982: Weddell Deep Water variability. *J. Mar. Res.,* **40,** 199–217.

——, 1991: Two stable modes of Southern Ocean winter stratification. *Deep Convection and Deep Water Formation in the Oceans,* P. C. Chu and J. C. Gascard, Eds., Elsevier Oceanography Series, Vol. 57, Elsevier, 17–35.

——, and B. A. Huber, 1984: Thermohaline stratification below the Southern Ocean sea ice. *J. Geophys. Res.,* **89** (C1), 641–648.

——, and J. C. Comiso, 1988: Polynyas in the Southern Ocean. *Sci. Amer.,* **256,** 90–97.

——, M. Visbeck, and J. C. Comiso, 2007: A possible link between the Weddell Polynya and the southern annular mode. *J. Climate,* **20,** 2558–2571.

Griffies, S. M., M. J. Harrison, R. C. Pacanowski, and A. Rosati, 2004: A technical guide to MOM4. GFDL Ocean Group Tech. Rep. 5, 295 pp.

Hallberg, R., and A. Gnanadesikan, 2006: The role of eddies in determining the structure and response of the wind-driven Southern Hemisphere overturning: Results from the Modeling Eddies in the Southern Ocean (MESO) project. *J. Phys. Oceanogr.,* **36,** 2232–2252.

Hibler, W. D., III, 1979: A dynamic thermodynamic sea ice model. *J. Phys. Oceanogr.,* **9,** 815–846.

Holland, D. M., 2001: Transient sea-ice polynya forced by oceanic flow variability. *Prog. Oceanogr.,* **28,** 403–460.

Killworth, P. D., 1979: On "chimney" formation in the ocean. *J. Phys. Oceanogr.,* **9,** 531–554.

——, 1983: Deep convection in the world ocean. *Rev. Geophys.,* **21,** 1–26.

Kuhlbrodt, T., R. S. Smith, Z. Wang, and J. M. Gregory, 2012: The influence of eddy parameterizations on the transport of the Antarctic Circumpolar Current in coupled climate models. *Ocean Modell.,* **52-53,** 1–8.

Large, W. G., J. C. McWilliams, and S. C. Doney, 1994: Oceanic vertical mixing: A review and a model with a vertical K-profile boundary layer parameterization. *Rev. Geophys.,* **32,** 363–403.

Lee, S.-K., W. Park, E. van Sebille, M. O. Baringer, C. Wang, D. B. Enfield, S. Yeager, and B. P. Kirtman, 2011: What caused the significant increase in Atlantic Ocean heat content since the mid-20th century? *Geophys. Res. Lett.,* **38,** L17607, doi:10.1029/2011GL048856.

Levitus, S., 1982: *Climatological Atlas of the World Ocean.* NOAA Prof. Paper 13, 173 pp. and 17 microfiche.

Locarnini, R. A., A. V. Mishonov, J. I. Antonov, T. P. Boyer, and H. E. Garcia, 2006: *Temperature.* Vol. 1, *World Ocean Atlas 2005,* NOAA Atlas NESDIS 61, 182 pp.

Maksym, T., and T. Markus, 2008: Antarctic sea ice thickness and snow-to-ice conversion from atmospheric reanalysis and passive microwave snow depth. *J. Geophys. Res.,* **113,** C02S12, doi:10.1029/2006JC004085.

Martin, T., W. Park, and M. Latif, 2012: Multi-centennial variability controlled by Southern Ocean convection in the Kiel Climate Model. *Climate Dyn.,* **40,** 2005–2022, doi:10.1007/s00382-012-1586-7.

Martinson, D. G., P. D. Killworth, and A. L. Gordon, 1981: A convective model for the Weddell Polynya. *J. Phys. Oceanogr.,* **11,** 466–488.

McDermott, D. A., 1996: The regulation of northern overturning by Southern Hemisphere winds. *J. Phys. Oceanogr.,* **26,** 1234–1255.

Murray, R. J., 1996: Explicit generation of orthogonal grids for ocean models. *J. Comput. Phys.,* **126,** 251–273.

Oke, P., and M. England, 2004: Oceanic response to changes in the latitude of the Southern Hemisphere subpolar westerly winds. *J. Climate,* **17,** 1040–1054.

Orsi, A. H., W. D. Nowlin, and T. Whitworth III, 1993: On the circulation and stratification of the Weddell gyre. *Deep-Sea Res.,* **40,** 169–203.

——, T. Whitworth III, and W. D. Nowlin, 1995: On the meridional extent and fronts of the Antarctic Circumpolar Current. *Deep-Sea Res.,* **42,** 641–673.

Ou, H. W., 1991: Some effects of a seamount on oceanic flows. *J. Phys. Oceanogr.,* **21,** 1835–1845.

Parkinson, C. L., and J. C. Comiso, 2008: Antarctic sea ice parameters from AMSR-E data using two techniques and comparisons with sea ice from SSM/I. *J. Geophys. Res.,* **113,** C02S06, doi:10.1029/2007JC004253.

Rahmstorf, S., 1993: A fast and complete convection scheme for ocean models. *Ocean Modell.,* **101,** 9–11.

——, and M. H. England, 1997: Influence of Southern Hemisphere winds on North Atlantic Deep Water flow. *J. Phys. Oceanogr.,* **27,** 2040–2054.

Smith, W. H. F., and D. T. Sandwell, 1997: Global seafloor topography from satellite altimetry and ship depth soundings. *Science,* **277,** 1957–1962.

Solomon, S., D. Qin, M. Manning, Z. Chen, M. Marquis, K. B. Averyt, M. Tignor, and H. L. Miller Jr., Eds., 2007: *Climate Change 2007: The Physical Science Basis.* Cambridge University Press, 996 pp.

Stössel, A., 2008: Employing satellite-derived sea ice concentration to constrain upper-ocean temperature in a global ocean GCM. *J. Climate,* **21,** 4498–4513.

Swart, N. C., and J. C. Fyfe, 2012: Observed and simulated changes in the Southern Hemisphere surface westerly wind-stress. *Geophys. Res. Lett.,* **39,** L16711, doi:10.1029/2012GL052810.

Thompson, D. W. J., and J. M. Wallace, 2000: Annular modes in the extratropical circulation. Part I: Month-to-month variability. *J. Climate,* **13,** 1000–1016.

Toggweiler, J. R., and B. Samuels, 1993: Is the magnitude of the deep outflow from the Atlantic Ocean actually governed by Southern Hemisphere winds? *The Global Carbon Cycle,* M. Heimann, Ed., Springer, 303–331.

——, and ——, 1995: Effects of Drake Passage on the global thermohaline circulation. *Deep-Sea Res.,* **42,** 477–500.

Wadhams, P., 2000: *Ice in the Ocean.* Gordon and Breach Science Publishers, 364 pp.

Whitworth, T., III, W. D. Nowlin, and S. J. Worley, 1982: The net transport of the Antarctic Circumpolar Current through Drake Passage. *J. Phys. Oceanogr.,* **12,** 960–971.

Winton, M., 2000: A reformulated three-layer sea ice model. *J. Atmos. Oceanic Technol.,* **17,** 525–531.

Zwally, H. J., and P. Gloersen, 1977: Passive microwave images of the polar regions and research applications. *Polar Rec.,* **18,** 431–450.